# Molecular-dynamics study of amorphization by introduction of chemical disorder in crystalline $NiZr_2$

C. Massobrio*
*Institut de Physique Expérimentale, Ecole Polytechnique Fédérale de Lausanne, PHB-Ecublens, CH-1015 Lausanne, Switzerland*

V. Pontikis† and G. Martin
*Section de Recherches de Métallurgie Physique, Centre d'Etudes Nucléaires de Saclay, 91191 Gif-sur-Yvette CEDEX, France*
(Received 20 December 1989)

By means of constant-temperature, constant-pressure molecular dynamics, we investigate the crystal-to-amorphous transformation of the intermetallic alloy $NiZr_2$ resulting from the introduction of antisite defects. We constructed an $n$-body potential in the framework of the second-moment approximation of the tight-binding description of the electronic density of states. This modeling of the interatomic forces is successful in reproducing both static and thermodynamic properties of the real material. The imposition of chemical disorder quantified by the appropriate value of the long-range-order parameter, $S$, engenders a volume expansion followed by relaxation to a stationary state characterized by lower density and higher potential energy. The behavior of the pair distribution functions, $g(r)$, reveals that amorphization takes place for values of $S \leq 0.6$, the corresponding volume expansion being of the order of 2%. Moreover the thermodynamic states obtained by chemical destabilization and rapid quenching from the liquid state are nearly identical. On the time scale of our simulations ($10^{-10}$ s), no detectable long-range diffusion of either species follows the introduction of chemical disorder. Some relevant features of the pair distribution functions (first and second peak positions, number of nearest neighbors) are in good agreement with those obtained experimentally from amorphous $NiZr_2$ samples generated by rapid quenching.

## I. INTRODUCTION

Amorphous metallic alloys can be produced by several experimental processes belonging to two distinct families: rapid quenching from a highly disordered (liquid or vapor) phase and crystal-to-amorphous ($C$-$A$) reactions in the solid state.[1] Rapid quenching prevents crystallization by bringing the material into a kinetically unfavorable condition. To avoid the nucleation and growth of more stable crystalline phases, cooling rates in the range $10^6$–$10^{12}$ K/s are typically employed. As a consequence the thickness of the material is rather small, of the order of 10–100 $\mu$m. For this reason it is of considerable interest to look for other ways of producing technologically useful bulk amorphous materials. In the case of $C$-$A$ reactions the methods of synthesis of amorphous solids are based on the existence of a driving force leading to the eventual disruption of the crystalline order. These transformations encompass solid-state reactions like multilayer interdiffusion, solid-gas reactions by hydrogen absorption or desorption, mechanical alloying, and irradiation-induced crystal destabilization.[2] In the first two cases the amorphization is due to an excess of free energy of the mixture formed from the pure elements with respect to the amorphous state of the same composition. In general the amorphous alloy will form preferentially because of the very different mutual diffusivities of the constituent elements preventing the formation of crystalline intermetallics.[3] The case studied by Yeh *et al.* is particularly instructive in this respect.[4] By hydriding crystalline $Zr_3Rh$ a two-phase reaction product, containing ZrH or $ZrH_2$ and some Rh-rich crystalline phases, is expected rather than a single-phase crystalline hydride which is too high in free energy. However, the formation of ZrH or $ZrH_2$ requires interdiffusion of Zr and Rh which cannot occur because of the reduced mobilities of the metal species. Therefore this "chemical frustration" effect suggested in Ref. 4 provides the mechanism for the transition to the glassy state, since this transition does not require an important interdiffusion of Zr and Rh. Amorphization by mechanical alloying has some similarities with multilayer interdiffusion since it is believed that the severe plastic deformation introduces point defects which may induce interdiffusion.[5] On the other hand, certain crystalline compounds can become amorphous when irradiated and destabilized at relatively low temperature depending on the system and the nature of the incident particles. Under these conditions the crystal-to-amorphous transformation of a chemically and topologically fully ordered alloy takes place as a reaction to the addition of some externally provided energy. This event leads to the actual loss of the crystalline structure and corresponds to a situation in which a highly energized material seeks a lower-energy state by transforming into a disordered structural arrangement. A global analysis of results of $C$-$A$ reactions indicates that chemical effects are crucial to the

 

production of highly energized states in a crystal. Evidence for this is mainly suggested by the presence of two or more different elemental species in most compounds undergoing amorphization in the solid state. According to Luzzi *et al.*,[6] chemical disorder appears to be the major driving force behind the *C-A* transition, at least in the case of electron irradiation, and it is likely that this form of excess energy plays a determinant role in the influence of analogous amorphization processes. This assertion is strengthened by the striking correlation existing between chemical disorder and the occurrence of amorphization found in Cu-Ti alloys.[7] In the compound $Cu_4Ti_3$, a critical temperature for chemical disordering exists and coincides with the critical temperature for amorphization. Above this critical temperature the effect of irradiation is limited to the production of secondary defects and the *C-A* transition is prevented. This result has been obtained via *in situ* measurements of the evolution of the Bragg-Williams long-range-order parameter $S$ with electron dose as a function of the temperature. Further experimental evidence supporting chemical disorder as the major driving force in the *C-A* transformation, at least in the case of irradiation-induced destabilization, is given by the Brillouin scattering and transmission electron microscopy studies of softening, disordering, and amorphization in $Zr_3Al$ performed by Okamoto, Rehn, and co-workers at Argonne National Laboratory (Argonne, IL).[8,9] This group established a close relationship between the critical dose of irradiation, the expansion of the lattice parameter ($\Delta V/V=2\%$), and the onset of amorphization corresponding to a threshold value $S=0.2$ of the long-range-order parameter. Moreover they proposed a parallelism between solid-state amorphization and melting based on the possibility that an elastic instability is involved in the transition. Along these lines Okamoto *et al.* conjectured that the volume dependence of the shear elastic constant associated with radiation-induced chemical disordering and eventual amorphization is essentially identical to that associated with the heating to melting of many solids. Given the above context we resorted to molecular-dynamics (MD) simulations to explore the role played by chemical disorder as driving force in the solid-state amorphization using an atomistic model well adapted to represent the static and dynamical properties of the alloy $NiZr_2$. $NiZr_2$ is particularly suited to our purposes because this material becomes amorphous not only by mechanical alloying[10] but also by electron irradiation.[11] This kind of external perturbation is exactly the one which is supposed to trigger the inception of chemical disorder. The primary purpose of this paper is therefore to study the influence of substitutional chemical disorder on the stability of crystalline $NiZr_2$. We rely on atomistic simulations because they are widely recognized as an excellent tool to achieve a better understanding of microscopic processes for which, as in the present case, rigorous and unambigous analytical foundations are lacking. Recent efforts in this direction have been reported by Limoge *et al.*,[12,13] who studied by molecular-dynamics simulation the amorphization of a pure Lennard-Jones system under the introduction of point defects, either Frenkel pairs or interstitials. This work was motivated by an early survey of irradiation amorphization by Limoge and Barbu,[14] who claimed interstitials to be the crucial defect responsible for amorphization. In analogy with experiments the results of Limoge *et al.* show clearly how the combined requirement of defect density and rate insertion of defects can preclude the amorphization in monoatomic metallic crystals. Due to the intrinsic flexibility of the simulations, these difficulties can be bypassed in a computer experiment as is done in Refs. 12 and 13. More recently Hsieh and Yip[15] extended the same idea to the case of a binary Lennard-Jones lattice in which the only difference between the two atomic species is the particle size. They found that the critical value of rate insertion and concentration of defects for the *C-A* reaction are much lower in binary than in monoatomic systems. Simulations of this kind based on Lennard-Jones potentials are certainly instructive but their interest is limited to a too qualitative and generic representation of phenomena which demands a careful establishment of the interatomic potential. To achieve this goal and to allow for a legitimate comparison with experiments we exercised great care in setting up a realistic $n$-body potential for $NiZr_2$, fitted to the alloy cohesive energy and elastic constants. The potential we elaborated is closely related to potentials recently constructed in the framework of the second-moment approximation to the tight-binding scheme of electronic density of states.[16] A number of investigations have shown that this family of potentials is successful in reproducing bulk and surface thermodynamical as well as structural properties of fcc metals.[17–19] The expression that we proposed is similar in spirit to those currently employed within the Daw-Baskes embedded-atom-method (EAM) scheme[20] but it necessitates a smaller number of adjustable parameters. This reduced flexibility does not affect the dynamical behavior of this potential which turns out to be very reliable when tested at high temperatures. Once we established the validity of the potential we set out to create in the lattice the microscopic conditions corresponding to chemical disorder. To this end we selected one configuration from the constant-temperature, constant-pressure molecular-dynamics trajectories for the system at equilibrium at $T=300$ K and we simply exchanged a given number of Ni and Zr particles chosen at random. The degree of chemical disorder is quantified in terms of the value taken by the long-range-order parameter $S$. The most convenient definition of $S$ for our purposes is given by $S=(p-r)/(1-r)$, where $p$ and $r$ are, respectively, the probability of presence of an $A$-type atom ($A$ = Ni or Zr) on an ordered lattice site and the molar ratio of $A$ atoms. By monitoring the pair distribution functions upon dynamical relaxation we witnessed the crystal-to-amorphous transformation for values of the long-range-order parameter $S \leq 0.6$.[21] On the other hand, the crystal is stable against introduction of chemical disorder when $S > 0.6$. Furthermore the amorphous pair distribution functions obtained by crystal destabilization are essentially identical to those resulting from a rapid quenching from the liquid state. Two additional aspects are worth noting, namely, the absence of long-range diffusion in the process of relaxation following disorder and the remark-

able agreement between the basic features of calculated and experimental pair distribution functions. Our results appear to validate the description of the *C-A* reaction proposed by Okamoto *et al.*[9] The transformation we observed resembles closely a first-order phase transformation provided one interprets the radiation-induced disordering as equivalent to an effective temperature rise and the threshold value of disorder as an effective melting point.

This paper is organized as follows. In Sec. II we describe the crystalline structure of the alloy chosen for our investigation, the interatomic potentials we used to model it, and the setup of our computations. Thermodynamic and structural features of the model before and after the imposition of chemical disorder are presented in Secs. III A and III B, respectively. Conclusive remarks are collected in Sec. IV.

## II. MODEL AND COMPUTATIONS

The crystalline structure of $NiZr_2$ is of the $CuAl_2$ ($C16$-structure) type depicted in Fig. 1. Each Ni atom has eight Zr atoms and two Ni atoms as nearest neighbors, the latter at a distance $d_{\text{Ni-Ni}}=c/2$ ($c$ being one of the cell lattice parameters) forming a linear chain. Each Zr atom has four Ni atoms as nearest neighbors and it is also surrounded by 11 other Zr atoms disposed at four slightly different distances.[22] An instructive way of looking at this structure is pointed out in Ref. 22: the Zr atoms form two sets of mutual orthogonal planes with a dense packing of hexagons parallel to (110) and ($1\bar{1}0$), respectively. The Ni atoms are situated in the channels parallel to the $c$ axis which are formed by this interlocking honeycomb structure (Fig. 1). A clear visual representation of the $NiZr_2$ spatial arrangement is also given in a paper by Visnov *et al.*[23] We studied systems of two different sizes: 108 Ni and 216 Zr atoms ($3\times3\times3$ lattice cells forming a parallelepipedic box) as well as 256 Ni and 512 Zr atoms ($4\times4\times4$ lattice cells). The exact positions of the atoms in the lattice cell as well as the lattice dimensions, $a=0.6483$ nm and $c=0.5267$ nm, are taken from Ref. 22. Crucial to a meaningful modeling of static and dynamical properties of materials is the choice of the interatomic potential. We related to a recent work on fcc transition metals[17] showing that a simple semiempirical tight-binding scheme based on the second-moment approximation to the electronic density of states can provide a good description of bulk and defect properties at zero temperature. As far as the dynamical behavior is concerned, Rosato *et al.*[17] stressed the importance of employing for the potential a cutoff radius which goes beyond nearest neighbors to achieve agreement between experimental and calculated mean-square displacements and thus avoid spurious effects of anharmonicity.[18,19] We follow closely these prescriptions and we employed the following expression for the cohesive energy:

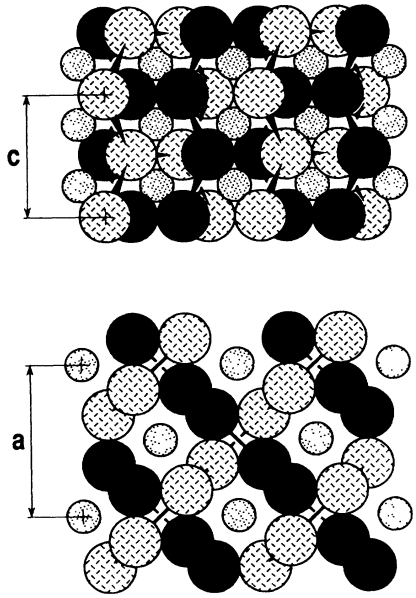


FIG. 1. The (001) (at the top of the figure) and the (100) (at the bottom) projections of the idealized $C16$-type structure of $NiZr_2$. The Ni atoms have been given a smaller diameter. Two different marks have been used for the Zr atoms to help distinguish between the Zr atoms lying in the (110) and ($1\bar{1}0$) hexagon networks.

$$E=\sum_{\alpha}\sum_{i_\alpha=1}^{N_\alpha}\left[\sum_{\beta}\sum_{\substack{j_\beta=1\\ j_\beta\neq i_\alpha}}^{N_\beta}A_{\alpha\beta}\exp\left[-p_{\alpha\beta}\left[\frac{r_{ij}^{\alpha\beta}}{d_{\alpha\beta}}-1\right]\right]-\left[\sum_{\beta}\sum_{\substack{j_\beta=1\\ j_\beta\neq i_\alpha}}^{N_\beta}\xi_{\alpha\beta}^2\exp\left[-2q_{\alpha\beta}\left[\frac{r_{ij}^{\alpha\beta}}{d_{\alpha\beta}}-1\right]\right]\right]^{1/2}\right] \tag{1}$$

where $r_{ij}^{\alpha\beta}=|r_{i\alpha}-r_{j\beta}|$ and the indexes $i_\alpha$ ($j_\beta$) run over all the particles. The repulsive portion is a Born-Mayer pairwise interaction and the attractive portion is the second-moment approximation of the tight-binding band energy.[16,17] Interactions have been computed for distances $r_{ij}^{\alpha\beta}$ within a spherical cutoff radius $r_c=0.53$ nm. We first decided to set $d_{\text{Ni-Ni}}$ and $d_{\text{Zr-Zr}}$ equal to the nearest-neighbor distances in pure Ni (Ref. 24) and Zr,[25] respectively, and $d_{\text{Ni-Zr}}$ equal to the nearest-neighbor distance in $NiZr_2$.[22] In the expression for the cohesive energy 12 parameters need to be determined. For the interaction between nickel atoms we simply referred to the values indicated in Ref. 17 where the potential accounts only for nearest neighbors. Then we proceeded similarly for the Zr-Zr interactions. We used the analytical form of Ref. 17 and we fitted a nearest-neighbor potential to experimental cohesive energy,[26] atomic volume, and elastic constants of pure zirconium.[27] At this stage the establishment of the potential necessitates the remaining four cross interaction parameters. These quantities are then fitted to the experimental cohesive energy, the bulk modulus,[28] and the atomic volume of $NiZr_2$. To get the

experimental cohesive energy of the alloy we added the formation enthalpy of crystalline $NiZr_2$ [$\Delta H_f = 0.39$ eV/atom (Ref. 29)] to the cohesive energy of an ideal mixture of $NiZr_2$, obtained by using the pure metal cohesive energies. The cutoff radius we adopted gives the best result in terms of a satisfactory overall agreement among all experimental and calculated elastic constants and it is sufficiently extended to avoid large discontinuities in the interatomic forces when a particle moves across it. However, we remark that there is a large difference between the elastic constant $C_{66}$ and the experimental value. The least-squares fit was performed by employing the software minimization package MERLIN (Ref. 30) and it led to a sum of squares equal to zero with an accuracy of seven digits. The equilibrium condition we imposed involves only the first derivative of the cohesive energy with respect to volume. As a consequence the three diagonal components of the stress tensor $\sigma_{ij}$ sum up to zero, but each one of them does not vanish. To correct this feature of our potential we maintained the above analytical form and minimized separately the diagonal components of the stress tensor by allowing for a variation of the $c$ and $a$ cell parameters. Table I collects the values of the potential parameters, together with the physical quantities used for the fit and gives a comparison between experimental and calculated elastic constants. In Table I are also included the values of the cell parameters corresponding to the two different fitting setups, referred to in the following as potential 1 (P1) and potential 2 (P2). We can anticipate that the two schemes will give the same results in terms of dynamical behavior of the potential and response to the introduction of chemical disorder. Our MD simulations are performed within the Nosé-Andersen constant-temperature, constant-pressure (*NPT*) technique[31,32] according to the equations of motion detailed elsewhere[33] and solved via a fifth-order predictor-corrector algorithm with time step $\Delta t = 10^{-15}$ s. Throughout this paper we used either cgs or reduced units defined as follows: $\sigma = 1$ Å for length, $\epsilon = 0.01$ eV $= 1.6 \times 10^{-14}$ erg for energy, $\tau = (m_{Ni}\sigma^2/\epsilon)^{1/2}$ for

TABLE I. Values of the tight-binding potential parameters for $NiZr_2$. The experimental values of cohesive energy $E_c$, bulk modulus $B$, and nearest-neighbor distances $\delta$, extrapolated at $T = 0$ K, are used for the fit of the potential parameters $p_{\alpha\beta}$, $q_{\alpha\beta}$, $A_{\alpha\beta}$, and $\xi_{\alpha\beta}$. The model parameters and the calculated elastic constants reported in the third column are those obtained by fitting the potential parameters to the experimental values of cohesive energy, bulk modulus, and cell dimensions $c$ and $a$ of $NiZr_2$. In the fourth column the cohesive energy, the bulk modulus, and the elastic constants were obtained upon minimization of the diagonal component of the stress tensor ($\sigma_{ij}$) with respect to $c$ and $a$. The calculated elastic constants are compared with the experimental values (in parentheses). $E_c$, $A_{\alpha\beta}$, and $\xi_{\alpha\beta}$ are expressed in eV/atom, elastic constants in units of $10^{12}$ dyn cm$^{-2}$, diagonal stress-tensor components of $NiZr_2$ in bars, and distances in nm. P1 and P2 denote the two fitting schemes adopted. The off-diagonal components of the stress tensor are zero for both schemes. The zero values are given with an accuracy of five digits.

| | Ni | Zr | $NiZr_2$ (P1) | $NiZr_2$ (P2) |
|---|---|---|---|---|
| $E_c$ | 4.44[a] | 6.17[b] | 6.0[c] | 5.9 |
| $B$ | 1.88[d] | 0.97[d] | 1.19[e] | 1.16 |
| $\delta$ | 0.249[a] | 0.318[f] | 0.2761[g] | 0.2761[g] |
| $C_{11}$ | 2.57(2.61[d]) | 1.53(1.55[d]) | 1.61(1.59[e]) | 1.47(1.59[e]) |
| $C_{12}$ | 1.65(1.51[d]) | 0.74(0.67[d]) | 1.05(1.34[e]) | 1.00(1.34[e]) |
| $C_{13}$ | | 0.55(0.65[d]) | 0.95(0.85[e]) | 0.95(0.85[e]) |
| $C_{33}$ | | 1.68(1.73) | 1.58(1.47[e]) | 1.67(1.47[e]) |
| $C_{44}$ | 0.93(1.32[c]) | 0.45(0.36) | 0.54(0.24[e]) | 0.54(0.24[e]) |
| $C_{66}$ | | | 0.61(0.06[e]) | 0.59(0.06[e]) |
| $p$ | 10.0 | 9.3 | 8.36 | 8.36 |
| $q$ | 2.7 | 2.1 | 2.23 | 2.23 |
| $A$ | 0.1368 | 0.1615 | 0.2166 | 0.2166 |
| $\xi$ | 1.756 | 2.34 | 2.139 | 2.139 |
| $\sigma_{xx}$ | | | 5760 | 0 |
| $\sigma_{yy}$ | | | 5760 | 0 |
| $\sigma_{zz}$ | | | −11 520 | 0 |
| $c$ | | | 0.5267[g] | 0.5124 |
| $a$ | | | 0.6483[g] | 0.661 08 |

[a]Reference 24.
[b]Reference 26.
[c]See text.
[d]Reference 27.
[e]Reference 28.
[f]Reference 25.
[g]Reference 22.

time, $T^*=k_BT/\epsilon$ for the temperature, $P^*=(\sigma^3/\epsilon)P$ for the pressure, and $D^*=(m_{Ni}/\epsilon\sigma^2)^{1/2}D$ for the diffusion coefficient. The pressure is also expressed in bars, where $P(\text{bars})=16\,000P^*$ and the stress-tensor components are given in units of pressure. In the above definitions $m_{Ni}$ is the nickel atomic mass, $k_B$ is the Boltzmann constant, and $V$ is the volume. Periodic boundary conditions are applied in the three directions. We assigned to the pseudomasses associated with the Nosé thermostat and the volume the values $Q^*=10$ and $W^*=10^4$, respectively. These have been kept constant throughout our simulations and no attempt has been made to adjust $W^*$ so as to optimize the relaxation time related to the equation of the volume.

To study the reaction of our system to substitutional chemical disorder we introduced antisite defects in one configuration pertaining to a well equilibrated trajectory at $T=300$ K according to the scheme of Fig. 2. In Fig. 2 the bidimensional lattice displayed is only intended to provide a simple example and does not represent the actual structure of $NiZr_2$. The long-range-order parameter $S=(p-r)/(1-r)$ can be defined in terms of two quantities, the probability $p$ of observing an atom $A$ on its original crystalline site and the molar ratio $r$ giving the percentage of $A$ atoms in the system. $S$ is equal to 1 for the chemically ordered crystalline structure and to zero when $p$ equals the molar ratio. It is simple to impose a certain degree of chemical disorder by keeping a Ni atom on its position in the crystal with a probability given by $p=r+S(1-r)$. First we generate a sequence of $N$ random numbers $\nu_n$ in between 0 and 1 ($N$ being the number of nickel atoms in the system). Next the position of the $n$th nickel atom is exchanged with the position of a randomly chosen zirconium atom provided $\nu_n$ is larger than the input probability $p$. We exercised care to avoid sampling a given Zr atom twice because in that case the exchange would not correspond to an increase of chemical disorder. Furthermore we made sure that the total number of exchanges corresponded to the input value of $S$. Then the system is allowed to evolve under the ($NPT$) dynamics with time step $\Delta t'=\Delta t/2$ at least for a few thousand time steps before restoring the original $\Delta t$. This reduction allows the algorithm to deal with the strong forces brought about by the spatial rearrangement that leads to amorphization.

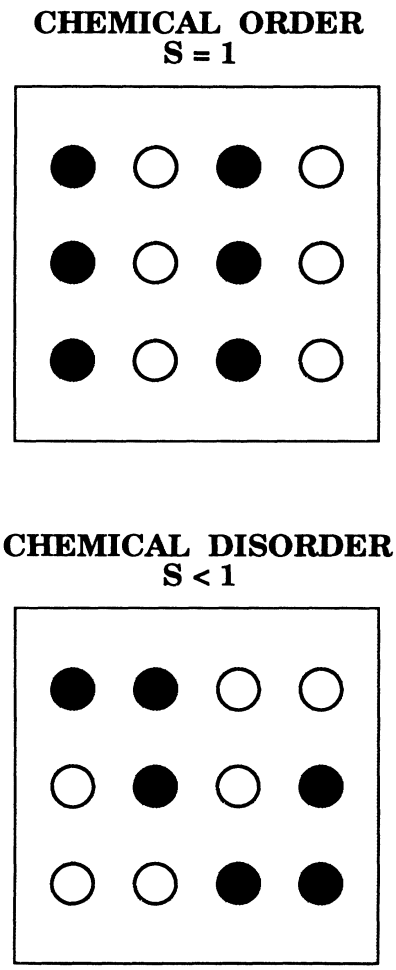


FIG. 2. Top part: schematic of a section of an $AB$ system chemically ordered ($S=1$) with atoms of both species on the crystalline positions. Bottom part: the same section of the $AB$ system upon introduction of chemical disorder.

Simulations lasted up to $2\times10^5$ time steps and were performed on two different computers: a Fujitsu FACOM VP-200 vectorial processor at the Centre Inte-Régional de Calcul Electronique (CIRCE) du Centre National de la Recherche Scientifique (CNRS), Orsay (France) and a Cray Research, Inc. Cray-2 supercomputer located at the Ecole Polytechnique Fédérale de Lausanne (Switzerland).

## III. RESULTS

### A. Equilibrium properties

We performed a series of simulations to establish the phase diagram of crystalline $NiZr_2$ and test the dynamical behavior of our model. In recent implementations of the EAM, an $n$-body potential scheme analogous to ours and widely employed to calculate properties of materials, the total energy of the lattice under uniform compression, and dilation was devised to obey the universal equation of state at zero temperature by Rose *et al.*[34] On the other hand, our potential does not account *a priori* for energy derivatives of order higher than second. Therefore it is of particular interest to know its ability to provide physically meaningful values of fundamental thermodynamical properties such as the thermal expansivity and the melting point. In Table II we present the values of volume, pressure, potential energy, and mean-square displacements at different temperatures for the two system sizes we studied. The same data are displayed in Fig. 3. We carried out constant-temperature, constant-pressure ($NPT$) simulations with the external pressure appearing in the temporal evolution of the volume set equal to zero. The truncation of the potential at $r_c=0.53$ nm brings about some difficulties in obtaining an average pressure

converging to the imposed one, especially at high temperature. This shortcoming may be corrected by resetting the imposed pressure to a suitable value.[35] We recorded high diffusion values of the order of $D=10^{-5}$ cm/s$^2$ at $T^*=13$ [the experimental melting point being equal tc $T^*=12.2$ ($T=1440$ K)] for the system of $N=768$ particles which melted after 200 000 time steps ($2\times10^{-10}$ s). In this case the second potential scheme (P2) was adopted. Similarly and for the first potential scheme (P1) 40 000 time steps were necessary to detect the occurrence of the crystal-liquid phase transition at $T^*=13.5$ with $N=768$. For the smaller system ($N=324$) melting occurred readily at $T^*=14$, the only temperature we investigated above $T^*=12$ for this system. Therefore we can conclude that the melting point of our model is located at a temperature $T_m^{\text{model}}\leq 13$. This estimate is consistent with the overheating that characterizes a model crystal in which extended defects are absent and the formation of Frenkel pairs is prevented because of their large formation energy and the limited duration of simulations. A stepwise increase of volume for $T^*>12$ is evident in our data for the volume-temperature phase diagram at zero imposed pressure displayed in Fig. 3. From this plot one deduces a thermal expansivity in between 1.5 and $2\times10^{-5}$ K$^{-1}$ in agreement with the value of $10^{-5}$ K$^{-1}$ quoted in Ref. 28. A similar picture of the phase transformation occurring at temperatures above $T^*=12$ is provided by the trend of the potential energy versus temperature also shown in Fig. 3. Further insight into the dynamical properties of our system can be gained by looking at the mean-square displacement $\langle u^2\rangle$ calculated along the $x$ direction. According to the Lindemann criterion the temperature of vibrational instability accompanying the melting of the crystal corresponds to a ratio $r=u/a$ equal to 0.1 where $u$ is the root-mean-square displacement and $a$ is the nearest-neighbor distance. Despite its empirical nature, the Lindemann criterion is roughly satisfied in a large variety of materials and gives a useful indication of the way a crystal is approaching the melting point. In our case the mean-square displacement at the experimental melting point is close to $0.06\times10^{-2}$ nm$^2$ and the corresponding Lindemann ratio is $r=u/a\approx0.08$ where, in this case, $a$ is the composition weighted average of nearest-neighbor distances in the pure metals. On the basis of these results and keeping in mind the poor value of $C_{66}$ at $T=0$ K, we conclude that the interatomic potential for $NiZr_2$ we devised is behaving well when tested against the experimental thermodynamical properties of $NiZr_2$. In fact it performs remarkably well at high temperatures despite its being fitted to static properties at $T=0$ K only. A comment is in order concerning the behavior of the stress-tensor components $\sigma_{ij}$ with temperature. Throughout the computations the values of the $\sigma_{ij}$ remained very close to

TABLE II. Values of the mean-square displacement $\langle u^2\rangle$, potential energy $U$, pressure $P$, and volume $V$ for crystalline $NiZr_2$ at temperatures ranging from 2 to 14 in reduced units ($\epsilon/k_B=115.88$ K). The data are averages calculated over $N_t$ time steps up to $T^*=12$. For the largest temperatures $N_t$ is the total length of the run leading eventually to melting and the averages reported are taken over the final portion of the trajectory ($10^4$ time steps equal $10^{-11}$ s). The imposed pressure is zero. $N$ is the number of particles, P1 and P2 denote the two fitting schemes for the potential, $\langle u^2\rangle$ is in units of $10^{-2}$ nm$^2$, $U$ in units of eV/mole, $V$ in units of cm$^3$/mole, pressure and temperature are in reduced units [$P$(bars)$=16\,000P^*$].

| $T^*$ | $N$ | $N_t$ | $\langle u^2\rangle$ | $U$ | $V$ | $P^*$ |
|---|---|---|---|---|---|---|
| 2 | 324(P1) | 8 000 | 0.010 | −17.68 | 33.78 | 0.03 |
| 2.6 | 324(P1) | 8 000 | 0.012 | −17.66 | 33.87 | 0.02 |
| 4 | 324(P1) | 8 000 | 0.016 | −17.56 | 34.12 | 0.11 |
| 6 | 324(P1) | 8 000 | 0.022 | −17.43 | 34.52 | 0.11 |
| 8 | 324(P1) | 8 000 | 0.033 | −17.30 | 34.99 | 0.08 |
| 10 | 324(P1) | 8 000 | 0.044 | −17.15 | 35.49 | 0.06 |
| 12 | 324(P1) | 8 000 | 0.054 | −17.00 | 36.04 | 0.11 |
| 14 | 324(P1) | 20 000 | | −16.54 | 37.53 | 0.16 |
| 2.6 | 768(P1) | 10 000 | 0.012 | −17.64 | 33.90 | 0.02 |
| 2.6 | 768(P2) | 8 000 | 0.010 | −17.66 | 33.83 | 0.07 |
| 4 | 768(P2) | 8 000 | 0.016 | −17.58 | 34.09 | 0.06 |
| 6 | 768(P1) | 10 000 | 0.027 | −17.43 | 34.49 | 0.18 |
| 6 | 768(P2) | 8 000 | 0.024 | −17.45 | 34.50 | 0.05 |
| 8 | 768(P2) | 8 000 | 0.036 | −17.32 | 34.89 | 0.11 |
| 9 | 768(P1) | 10 000 | 0.042 | −17.22 | 35.24 | 0.08 |
| 12 | 768(P1) | 10 000 | 0.063 | −16.97 | 36.22 | −0.09 |
| 12 | 768(P2) | 22 000 | 0.058 | −17.03 | 35.84 | 0.19 |
| 13 | 768(P2) | 200 000 | | −16.65 | 36.95 | 0.29 |
| 13.5 | 768(P1) | 40 000 | | −16.68 | 36.98 | 0.20 |
| 13.5 | 768(P2) | 72 000 | | −16.60 | 37.24 | 0.16 |

TABLE III. Thermodynamic quantities calculated for the rapid quench liquid to glass simulations. The starting point is a configuration of the liquid at $T^*=13.4$ ($N=768$). The quenching rate is $4.2\times10^{13}$ K/s. $T_{in}$ is the temperature of the system at the beginning of each run and $T_f$ is the thermostat temperature. $\Delta N_s$ is the length of the quenching step in $\Delta t$ ($\Delta t=10^{-15}$ s). At $T^*=2.6$ the system is annealed at constant temperature for 60 000 time steps. $V$ is the volume averaged over $\Delta N_s$ time steps, similarly $U$ is the potential energy and $P$ the calculated pressure (the imposed pressure being zero). $U$ is given in eV/mole, $V$ in cm$^3$/mole, $P$ and $T$ in reduced units.

| $T^*_{in}$ | $T^*_f$ | $\Delta N_s$ | $V$ | $U$ | $P^*$ |
|---|---|---|---|---|---|
| 13.4 | 9.8 | 10 000 | 36.21 | −16.88 | 0.14 |
| 9.8 | 6.2 | 10 000 | 35.26 | −17.16 | 0.14 |
| 6.2 | 2.6 | 10 000 | 34.58 | −17.39 | 0.06 |
| 2.6 | 2.6 | 60 000 | 34.51 | −17.41 | 0.06 |

those imposed by the fitting schemes for the ideal crystal relaxed at zero temperature and pressure as detailed in Sec. II. Therefore the model does not exhibit any tendency toward a crystalline structural transformation with increasing $T$. We devoted a separate set of computations relating to this problem by performing simulations within the Parrinello-Rahman scheme.[36,37] This implementation accounts for temporal variation of the shape and the size of the system box in response to any imbalance between the internal and external pressure.

Finally we focused on the properties of the glass produced by rapid quenching of the melt. Starting from a configuration inherent to the melt at $T^*=13.4$ we cooled the system down to room temperature at a quenching rate equal to $4.2\times10^{13}$ K/s. The details of the cooling schedule and the thermodynamic quantities relative to these simulations are shown in Table III. The path we followed mimics the experimental rapid quenching scheme by which a glass is produced through the introduction of kinetic constraints inhibiting the crystallization. At $T^*=2.6$ ($T=300$ K) we annealed the system for 60 000 time steps and we characterized the thermodynamic state by calculating the pair distribution functions $g(r)$. This step is of fundamental interest because it allows a direct comparison with the analogous results we obtain by crystal-to-amorphous transformations induced by chemical disorder. We shall come back to this issue shortly.

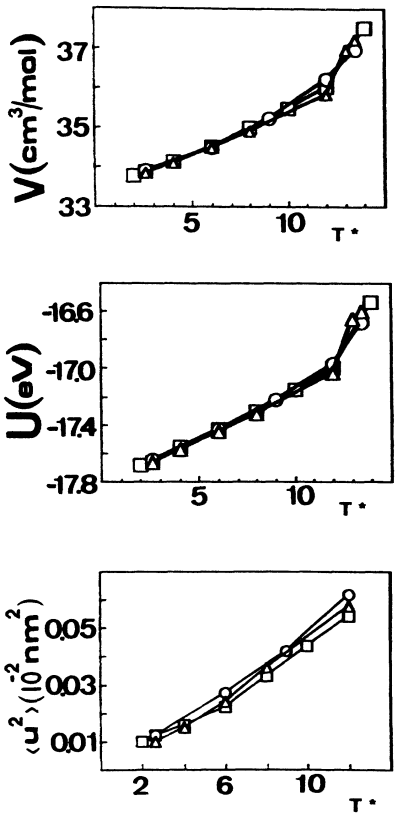


FIG. 3. From top to bottom: variation of volume $V$, potential energy per mole $U$, and mean-square displacements in $NiZr_2$ as a function of temperature (in reduced units, see text) for the three different system sizes and/or interatomic potentials we studied. Open square, $N=324$; open circle, $N=768$ and potential P1; open triangle, $N=768$ and potential P2.

### B. Response to chemical disorder

The introduction of chemical disorder has the primary effect of causing a volume increase of the system which relaxes to a stationary situation with negligible changes in the values of thermodynamical and structural quantities throughout the length of our simulations ($10^{-10}$ s). This effect is illustrated in Fig. 4 where we plot the average volume at $T=300$ K ($N=324$) over a time interval that includes the equilibrium portion of the run and the phases of over expansion and relaxation of the crystal brought about by the presence of antisite defects. Table IV gives the largest average volumes as well as the values recorded after 5000 $\Delta t$, 10 000 $\Delta t$, and at the end of the

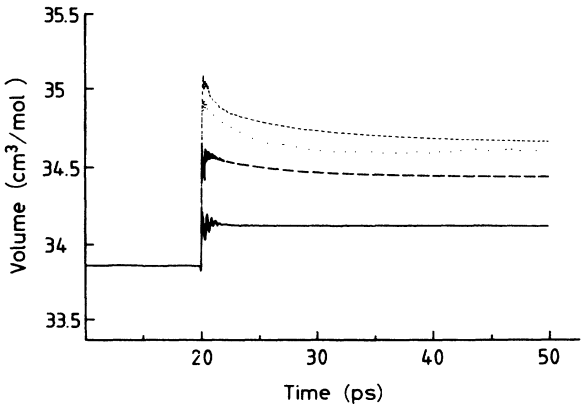


FIG. 4. Average volume of the system at $T=300$ K before and after introduction of chemical disorder. Solid line, $S=0.9$; dashed line, $S=0.6$; dotted line, $S=0.2$; short-dashed line, $S=0$.

TABLE IV. Average volumes and potential energies for two different system sizes following the introduction of chemical disorder in $NiZr_2$. $S$ is the long-range-order parameter, $N$ the number of particles, $N_S$ the total duration of the run, $V$ the average volume over the time interval given in parentheses ($t=0$ denoting the onset of chemical disorder), $V_{max}$ the largest $V$ attained, $\Delta V/V_{eq}$ the volume expansion with respect to the equilibrium value, $U$ the potential energy averaged over $N_S$ time steps. $V$ is in units of $cm^3$/mole, $U$ of eV/mole, $\Delta t$ is equal to $10^{-15}$ s.

| $S$ | $N$ | $N_S$ | $V_{max}$ | $V$ $(5000\,\Delta t)$ | $V$ $(10^4\,\Delta t)$ | $V$ $(N_S\,\Delta t)$ | $\Delta V/V_{eq}$ | $U$ |
|---|---|---|---|---|---|---|---|---|
| 0 | 324 | 40 000 | 35.08 | 34.79 | 34.73 | 34.65 | 0.024 | −17.37 |
| 0.2 | 324 | 40 000 | 34.92 | 34.68 | 34.63 | 34.60 | 0.021 | −17.38 |
| 0.4 | 324 | 40 000 | 34.76 | 34.59 | 34.57 | 34.53 | 0.019 | −17.40 |
| 0.6 | 324 | 40 000 | 34.60 | 34.50 | 34.46 | 34.43 | 0.016 | −17.41 |
| 0.9 | 324 | 40 000 | 34.22 | 34.13 | 34.13 | 34.12 | 0.007 | −17.54 |
| 0 | 768 | 220 000 | 34.98 | 34.66 | 34.66 | 34.53 | 0.021 | −17.40 |
| 0.5 | 768 | 140 000 | 34.81 | 34.57 | 34.57 | 34.43 | 0.018 | −17.40 |
| 0.6 | 768 | 140 000 | 34.73 | 34.55 | 34.55 | 34.45 | 0.018 | −17.43 |
| 0.7 | 768 | 140 000 | 34.53 | 34.47 | 34.47 | 34.39 | 0.017 | −17.45 |

simulations that lasted $2.2\times10^{-10}$ s at most for $S=0$, $N=768$ ($N_S=220\,000$). Systems of two sizes were considered ($N=324$ and $N=768$) and the potentials P1 and P2 were employed, respectively. We measure time intervals in units of $\Delta t=10^{-15}$ s but we employed also $\Delta t'=0.5\times10^{-15}$ s for a few thousand time steps just after the introduction of the Ni-Zr exchanges as mentioned in Sec. II. We included also in Table IV the potential energy $U$ and the volume expansion $\Delta V/V_{eq}$ measured upon relaxation with respect to the crystal at equilibrium. The values of $\Delta V/V_{eq}$ are quite similar for long-range-order parameters in between 0 and 0.7; less important is the expansion induced in the case $S=0.9$ corresponding to only 9 Ni-Zr exchanges for a system composed of 108 Ni and 216 Zr atoms. Table IV shows that the largest volume reduction in the interval between $5000\,\Delta t$ and $N_S\,\Delta t$ is 0.4% and 0.25% in between $10\,000\,\Delta t$ and $N_S\,\Delta t$. We conclude that the length of the transient stage following the onset of the perturbation is not more extended than $20\,000\,\Delta t$. Furthermore the states obtained by chemical disorder (except in the case of $S=0.9$) and rapid quenching of the liquid down to room temperature yield quite similar potential energies and atomic volumes, as exhibited in Tables III and IV.

A microscopic insight into the response of the system is given by the temporal evolution of the mean-square displacement $\langle\delta r^2\rangle$ calculated for Ni and Zr separately. Figure 5 shows the trend of $\langle\delta r^2\rangle$ in the case of $S=0$, $N=768$ and indicates that during the first 10 000 steps the atoms seek a local rearrangement with an apparent diffusion coefficient of the order of $10^{-6}$ $cm^2/s$. On the other hand, the $\langle\delta r^2\rangle$ independently averaged over two subsequent runs of 10 000 and 20 000 steps each are limited to less than $0.1\times10^{-2}$ $nm^2$. This result demonstrates that no long-range diffusion of either atomic species detectable on the time scale of our simulations follows the introduction of chemical disorder.

Pair distribution functions $g(r)$ are the appropriate quantities to detect structural changes occurring in a crystalline structure. The computation of the $g(r)$ for each value of $S$ can help to find the threshold value of chemical disorder necessary for the system to leave the crystalline portion of the phase diagram and reach isothermally a metastable situation characterized by higher potential energy and a loss of topological order. We calculated the $g(r)$ periodically over segments of 10 000 time steps for both system sizes and all values of $S$. The shapes of the pair distribution functions obtained by averaging, respectively, over the time interval $(10\,000-20\,000)\Delta t$ after the introduction of chemical disorder and a last segment of 10 000 time steps are indistinguishable. This confirms our previous statement on the length of the transient stage ($\approx20\,000$ steps). On the basis of these considerations when referring to a pair dis-

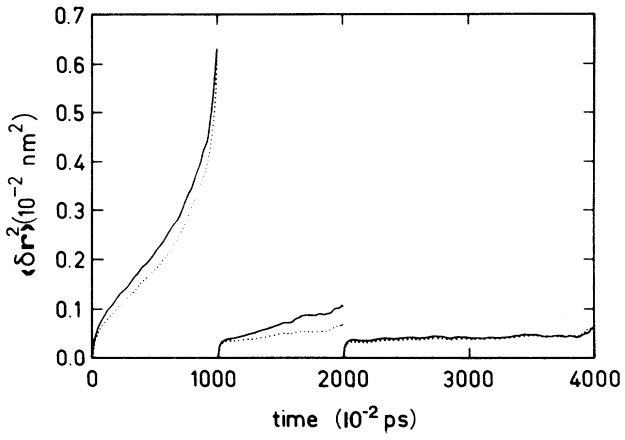


FIG. 5. Temporal evolution of the mean-square displacements of Ni atoms (solid line) and Zr atoms (dotted line) after the introduction of chemical disorder ($S=0$). The graph shows three independent averages taken over the intervals $(0-10\,000)\Delta t$, $(10\,000-20\,000)\Delta t$, and $(20\,000-40\,000)\Delta t$.

tribution function $g(r)$ we shall imply hereafter quantities averaged over the final 10 000 time steps of the trajectory and mostly for the largest system, except in one case, $S=0.9$ when we used $N=324$ atoms. The transformation from the crystalline to the amorphous state is highlighted by the evident structural differences existing between the pair distribution functions [global and restricted to interactions between like (Ni-Ni, Zr-Zr) and unlike (Ni-Zr) atoms] of $NiZr_2$ computed before and after the imposition of the largest degree of chemical disorder (see Figs. 6 and 7). Also in Figs. 6 and 7 we plotted the $g(r)$ of the structure obtained by rapidly quenching the liquid. The disordered states obtained by chemical destabilization and rapid cooling from the liquid state (we denote them $AC$ and $AL$) feature global $g(r)$ nearly identical as expected in view of the values of the corresponding thermodynamic quantities. On the other hand, the Ni-Ni pair distributions differ somewhat in shape, particularly in between 0.4 and 0.6 nm. Less dramatic are the differences in the cross distribution functions and the two $g(r)$ relative to interactions among Zr atoms are essentially identical. We notice also that in the case of cross interactions the first peak is lower and the second peak is farther apart and less pronounced in the $AL$ than in the $AC$ case (Fig. 7). By taking the integral of the Ni-Ni $g(r)$ up to the first minimum we obtain coordination numbers equal to 2 for the crystal, 2.75 for $AC$, and 3.72 for $AL$. These peculiarities suggest that the nickel atoms stow more compactly at short distances in the amorphous structure and particularly when it originates from the liquid state. For zirconium the coordination number decreases from 11 in the crystal to 10.5 in both amorphous structures. Therefore the rearrangement imposed by the chemical disorder affects more heavily the nickel than the zirconium atoms. Similar features were found in the experimental partial pair distribution functions obtained by neutron diffraction on samples of $Ni_{36}Zr_{64}$ prepared by rapid quenching from the liquid state. By Fourier transforming the partial interference functions $S(Q)$ Mizoguchi *et al.*[38] concluded that in amorphous $Ni_{36}Zr_{64}$ a nickel atom has an average of 3.3 nickel atom nearest neighbors, while for zirconium the same quantity is equal to

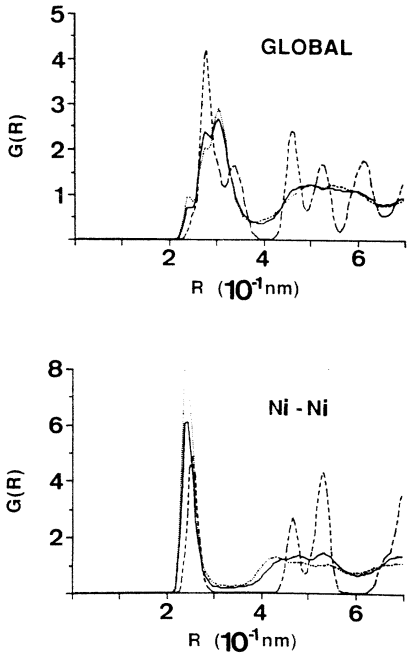


FIG. 6. Global and partial Ni-Ni pair distribution functions at $T=300$ K. Dashed line: crystalline $NiZr_2$ Solid line: after the imposition of chemical disorder, $S=0$. Dotted line: amorphous obtained by rapid quench from the liquid state.

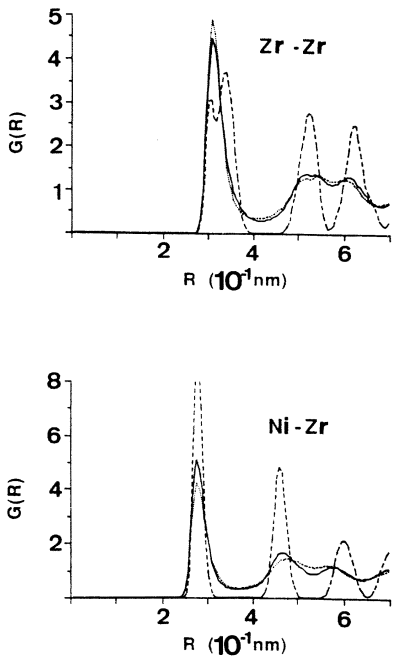


FIG. 7. Partial Zr-Zr and cross pair distribution functions at $T=300$ K. Dashed line: crystalline $NiZr_2$. Solid line: after the imposition of chemical disorder, $S=0$. Dotted line: amorphous obtained by rapid quench from the liquid state.

TABLE V. Position of first and second maximum, first minimum, and number of nearest neighbors NN in the amorphous $NiZr_2$ corresponding to a degree of chemical disorder $S=0$ for $N=768$ atoms. Distances are given in nm. Experimental values are in parentheses.

| | 1st maximum | 1st minimum |
|---|---|---|
| Ni-Ni | 0.24 (0.245;[a] 0.266[b]) | 0.33 (0.335;[a] 0.330[b]) |
| Zr-Zr | 0.31 (0.330;[a] 0.315[b]) | 0.42 (0.425;[a] 0.040[b]) |
| Ni-Zr | 0.28 (0.285;[a] 0.269[b]) | 0.37 (0.40[a]) |
| | **2nd maximum** | **No. of NN's** |
| Ni-Ni | 0.47 (0.40[a]) | 2.75 (3.3;[a] 2.3[b]) |
| Zr-Zr | 0.52 (0.52[a]) | 10.50 (11;[a] 9[b]) |
| Ni-Zr | 0.46 (0.44[a]) | 7.80 (8.6;[a] 5.6[b]) |
| Zr-Ni | | 3.90 (4.8;[a] 2.9[b]) |

[a]Reference 38.
[b]Reference 39.

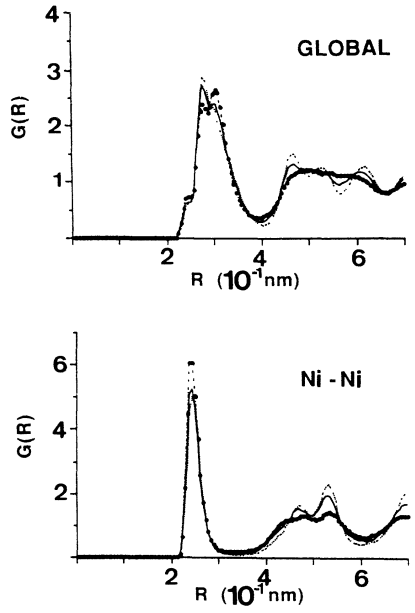


FIG. 8. Global and partial Ni-Ni pair distribution functions for three different degrees of chemical disorder at $T=300$ K. Dashed-dotted thick line: $S=0$. Solid line: $S=0.6$. Dotted line: $S=0.7$.

the value taken in the crystal. Further measurements performed by Lee *et al.*[39] on $Ni_{35}Zr_{65}$ employing x-ray and neutron techniques give smaller coordination numbers for both species. Table V shows the remarkable overall agreement between measured and calculated first and second peak positions of partial $g(r)$. Table V gives also the position of the first minimum of partial $g(r)$ and the coordination numbers.

By increasing $S$ some signatures of the crystalline structure appear in the Ni-Ni pair distribution function beginning for $S=0.5$ and more clearly for $S=0.6$ and $S=0.7$ as shown in Fig. 8. Negligible changes are detected for $S=0.2$ and $S=0.4$. In the bottom part of Fig. 8 relative to the Ni-Ni $g(r)$ for $S=0.6$ and $S=0.7$ one notices two peaks developing out of the second shell of neighbors, the first lower than the second as in the unperturbed lattice. At $S=0.6$ the first peak of the global $g(r)$ becomes for the first time more prominent than the one located immediately at its right. This feature is characteristic of the crystalline solid (Fig. 8, top part). We believe this signature can provide a simple criterion to mark the boundary between crystalline and amorphous material. More reminiscent of the crystal are also the Zr-Zr and cross pair distribution function displayed in Fig. 9. The structures obtained for $S=0.7$ are even more crystal-like either regarded through the behavior of the global or partial $g(r)$, all of them strongly resembling the analogous quantities calculated for the equilibrium structure. For $S=0.9$ (Fig. 10) the shapes of the global and Ni-Ni pair distribution functions confirm that this amount of chemical disorder does not induce the crystal-to-amorphous transition.

Finally we recall that the behavior of the stress-tensor components $\sigma_{ij}$ was carefully monitored throughout the

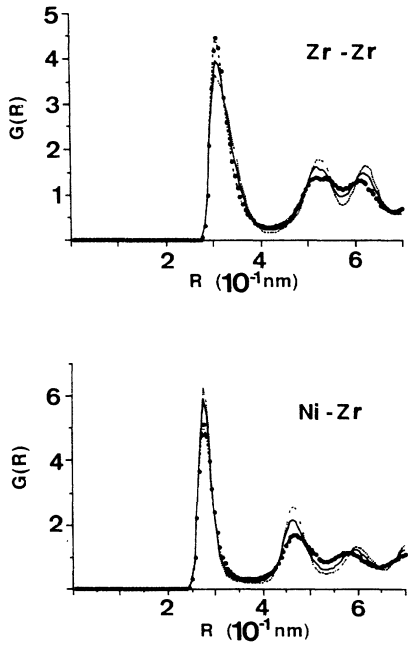


FIG. 9. Partial Zr-Zr and cross pair distribution functions for three different degrees of chemical disorder at $T=300$ K. Dash-dotted thick line: $S=0$. Solid line: $S=0.6$. Dotted line: $S=0.7$.

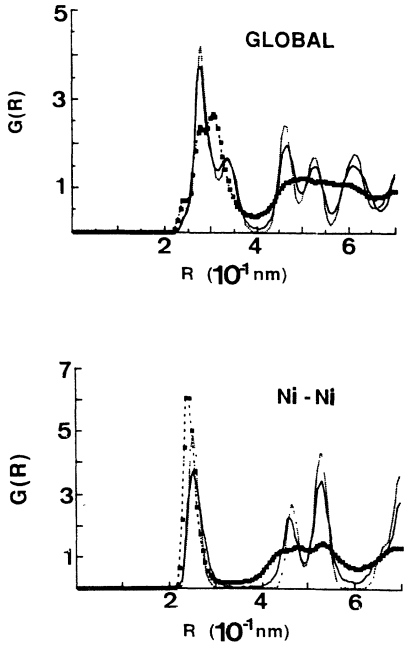


FIG. 10. Global and partial Ni-Ni pair distribution functions at $T=300$ K for two different degrees of chemical disorder ($S=0.9$ and $S=0$) and the crystalline state. Dotted line: crystalline $NiZr_2$. Solid line: $S=0.9$. Dash-dotted thick line: $S=0$.

computations performed after the introduction of chemical disorder. We recorded moderate changes in the values of the off-diagonal $\sigma_{ij}$ amounting to a few kilobars. Since the transition we were interested in is an order-disorder one and the transformation toward the amorphous state manifested readily we believe the use of a simulation box of fixed form did not alter the substance of our results. Further support to this conjecture is given by a separate set of computations performed within the Parrinello-Rahman scheme.[37]

## IV. CONCLUSIONS

The main purpose of this paper is to investigate by molecular-dynamics simulations the effects of the presence of antisite defects on the stability of crystalline $NiZr_2$. We focused on chemical disorder because this form of storage of external energy is believed to play an important role in most crystal-to-amorphous reactions, particularly in the case of electron induced destabilization. We constructed an $N$-body potential and we checked its reliability against experimental static and thermodynamical properties of the alloy obtaining very reasonable values for thermal expansivity, mean-square displacements, and melting temperature. A moderate degree of chemical disorder is sufficient to induce the crystal-to-amorphous transformation. Already for $S=0.7$ the shape of the global pair distribution function differs radically from the one relative to the crystal. Volume expansion and potential energy indicate the achievement of a stationary state accompanied by a conspicuous loss of topological order. However, we believe the transformation is not complete for $S=0.7$ and the simple criterion we proposed in Sec. III B referring to the heights of the first two peaks of the global $g(r)$ points toward $S=0.6$ as threshold value for the $C$-$A$ reaction. The volume expansion associated with amorphization is of the order of 2%, it decreases slowly going from $S=0$ to $S=0.7$, and becomes less than 1% for a degree of disorder ($S=0.9$) that does not destabilize the crystal. Unlike the erroneously reported values in Ref. 21, the volume expansion at the critical level of chemical disorder $S=0.6$ is 1.6% for $N=768$ and 1.7% for $N=324$ and therefore similar to the one that triggers the onset of amorphization in the compound $Zr_3Al$. The data displayed in Table IV and the results on $Zr_3Al$ lend support to the conjecture that a value of $\Delta V/V_{eq}$ not too different from 2% might represent a universal threshold of instability beyond which an intermetallic alloy loses its topological order. Concerning the nature of the $C$-$A$ transition our results validate the interpretation formulated by Okamoto *et al.*[9] suggesting an analogy between amorphization by chemical disorder and melting. In our case volume and potential energy are close to those of the crystal for $S=0.9$, change abruptly already for $S=0.7$, and remain essentially constant down to $S=0$. The global pair distribution functions provide striking and unambiguous evidence that topological disorder sets in beginning from $S=0.6$ without further dramatic changes for smaller values of $S$. It is therefore tempting to conclude that raising the degree of chemical disorder corresponds to an effective temperature rise and the critical degree of chemical disorder is associated with drastic thermodynamical and structural changes analogous to those occurring at the melting point. Work is in progress to investigate the response of the same model to the imposition of a nonhomogeneous form of chemical disorder, namely, localized on an internal portion of the system surrounded by a region free of defects. In the context of $C$-$A$ reactions computations are under way to highlight the influence of extended defects as grain boundaries on the process of nucleation of the amorphous phase.

## ACKNOWLEDGMENTS

This work started during a stay of C.M. at the Centre d'Etudes de Chimie Métallurgique (CECM) du Centre National de la Recherche Scientifique (CNRS) Vitry-sur-Seine (France) and continued when C.M. was at the Institut de Physique Expérimentale (IPE) de l'Ecole Polytechnique Fédérale de Lausanne (Switzerland) while supported by the Swiss National Science Foundation. J. P. Chevalier, director of CECM, and other members of CECM are thanked for their encouragement and support. C.M. is also grateful to Professor J. Buttet, director of IPE for his constant interest in this work, to B. Hall and C. L. Bandelier for technical assistance, and to Dr. W. de Heer for a critical reading of the manuscript. We also acknowledge fruitful discussions with J. C. De Lima at Laboratoire pour l'Utilisation du Rayonnement Electromagnétique (LURE), Orsay (France).

*Present address: Composés non-stœchiométriques, CNRS, Université de Paris–Sud, Centre d'Orsay, Bâtiment 415, 91405 Orsay CEDEX, France.

†To whom correspondence should be addressed.

[1]R. B. Schwarz, W. L. Johnson, J. Less-Common Met. **140**, 1 (1988).

[2]W. L. Johnson, Prog. Mater. Sci. **30**, 81 (1986).

[3]M. Gerl and P. Guilmin, Solid State Phenomena **3-4**, 215 (1988).

[4]X. L. Yeh, K. Samwer, and W. L. Johnson, Appl. Phys. Lett. **42**, 243 (1983).

[5]P. Y. Lee, J. Jang, and C. C. Koch, J. Less-Common Met. **140**, 73 (1988).

[6](a) D. E. Luzzi, H. Mori, H. Fujita, and M. Meshii, Scr. Metall. **19**, 798 (1985); (b) D. E. Luzzi, H. Mori, H. Fujita, and M. Meshii, Acta Metall. **34**, 629 (1986).

[7]D. E. Luzzi and M. Meshii, Res. Mechanica **21**, 207 (1987).

[8]L. E. Rehn, P. R. Okamoto, J. Pearson, R. Bhadra, and M. Grimsditch, Phys. Rev. Lett. **59**, 2987 (1987).

[9]P. R. Okamoto, L. E. Rehn, J. Pearson, R. Bhadra, and M. Grimsditch, J. Less-Common Met. **140**, 231 (1988).

[10]H. Bakker, P. I. Loeff, and A. W. Weeber, Defect Diffusion Forum **66-69**, 1169 (1989).

[11]H. Mori, H. Fujita, M. Tendo, and M. Fujita, Scr. Metall. **18**, 783 (1984).

[12]Y. Limoge, A. Rahman, H. Hsieh, and S. Yip, J. Non-Cryst. Solids **99**, 75 (1988).

[13]H. Hsieh and S. Yip, Phys. Rev. Lett. **59**, 2760 (1987).

[14]Y. Limoge and A. Barbu, Phys. Rev. B **30**, 2212 (1984).
[15]H. Hsieh and S. Yip, Phys. Rev. B **39**, 7476 (1989).
[16]F. Ducastelle, J. Phys. (Paris) **31**, 1055 (1970).
[17]V. Rosato, M. Guillope, and B. Legrand, Philos. Mag. A **59**, 321 (1989).
[18]M. Guillope and B. Legrand, Surf. Sci. **215**, 577 (1989).
[19]B. Loisel, D. Gorse, V. Pontikis, and J. Lapujoulade, Surf. Sci. **221**, 365 (1989).
[20]M. S. Daw and M. I. Baskes, Phys. Rev. B **29**, 6443 (1984).
[21]C. Massobrio, V. Pontikis, and G. Martin, Phys. Rev. Lett. **62**, 1142 (1989).
[22]E. E. Havinga, H. Damsa, and P. Hokkeling, J. Less-Common Met. **27**, 169 (1972).
[23]R. Visnov, F. Ducastelle, and G. Treglia, J. Phys. F **12**, 441 (1982).
[24]C. Kittel, *Introduction à la Physique de l'État Solide,* 2nd ed. (Dunod, Paris, 1972).
[25]A. R. Kaufmann and T. T. Magel, in *Metallurgy of Zirconium,* edited by B. Lustman and F. Kerze (McGraw-Hill, New York, 1955), p. 377.
[26]G. B. Skinner, J. W. Edwards, and H. L. Johnson, J. Am. Chem. Soc. **73**, 174 (1951).
[27]G. Simmons and H. Wang, *Single Crystal Elastic Constants and Calculated Aggregates Properties* (MIT Press, Cambridge, Mass., 1971).
[28]F. R. Eshelman and J. F. Smith, J. Appl. Phys. **46**, 5080 (1975).
[29]M. P. Henaff, C. Colinet, A. Pasturel, and K. H. J. Buschow, J. Appl. Phys. **56**, 307 (1984).
[30]G. A. Evangelakis, J. P. Rizos, I. E. Lagaris, and I. N. Demetropoulos, Comput. Phys. Commun. **46**, 401 (1987).
[31]S. Nosé, J. Chem. Phys. **72**, 2384 (1980).
[32]H. C. Andersen, J. Chem. Phys. **72**, 2384 (1980).
[33]C. Massobrio, V. Pontikis, and G. Ciccotti, Phys. Rev. B **39**, 2640 (1989).
[34]J. H. Rose, J. R. Smith, F. Guinea, and J. Ferrante, Phys. Rev. B **29**, 2963 (1984).
[35]M. Ferrario and J. P. Ryckaert, Mol. Phys. **53**, 587 (1985).
[36]M. Parrinello and A. Rahman, J. Appl. Phys. **52**, 7182 (1981).
[37]C. Massobrio, V. Pontikis, and F. Willaime (unpublished).
[38]T. Mizoguchi, S. Yoda, N. Akutsu, S. Yamada, J. Nishioka, T. Suemasa, and N. Watanabe, in *5th International Conference on Rapidly Quenched Metals,* Würzburg, Germany, 1984, edited by F. Steeb and H. Warlimont (North-Holland, Amsterdam, 1985), p. 483.
[39]A. Lee, G. Etherington, and C. N. J. Wagner, J. Non-Cryst. Solids **61-62**, 349 (1984).

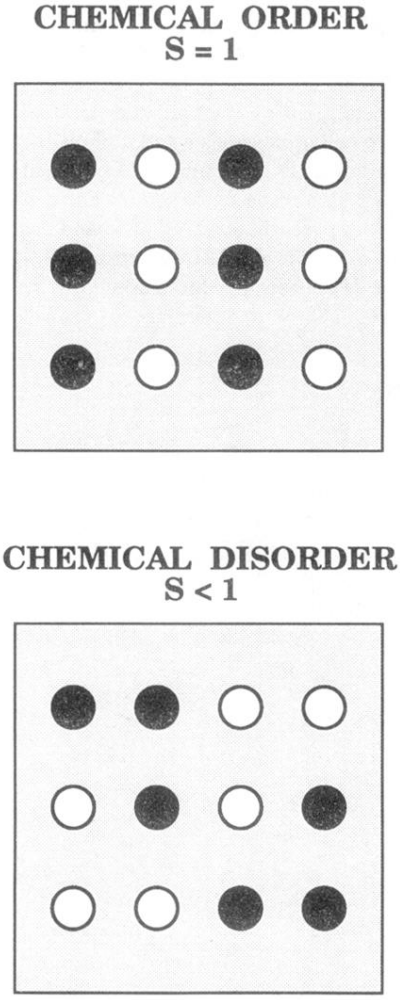


FIG. 2. Top part: schematic of a section of an $AB$ system chemically ordered ($S=1$) with atoms of both species on the crystalline positions. Bottom part: the same section of the $AB$ system upon introduction of chemical disorder.